[8]L. R. Edwards and S. Legvold, Phys. Rev. 176, 753 (1968).
[9]W. J. Nellis and S. Legvold, Phys. Rev. 180, 581 (1969).
[10]A. R. Mackintosh, Phys. Rev. Letters 9, 90 (1962).
[11]R. J. Elliott and F. A. Wedgewood, Proc. Phys. Soc. (London) 81, 846 (1963).
[12]H. Miwa, Progr. Theoret. Phys. (Kyoto) 29, 477 (1963).
[13]A. J. Freeman, J. O. Dimmock, and R. E. Watson, Phys. Rev. Letters 16, 94 (1966).
[14]G. S. Anderson and S. Legvold, Phys. Rev. Letters 1, 322 (1958).
[15]A. R. Mackintosh and F. A. Smidt, Phys. Letters 2, 107 (1962).

PHYSICAL REVIEW B VOLUME 3, NUMBER 5 1 MARCH 1971

Origin of the Magnetic "Surface Anisotropy" of Thin Ferromagnetic Films

Alan J. Bennett and Bernard R. Cooper
General Electric Research and Development Center, Schenectady, New York 12301
(Received 20 July 1970)

A very thin crystal (i. e., single-crystal film) of a cubic metal such as nickel is no longer truly cubic. This departure from cubic symmetry is reflected in the nature of the electronic states. We study the appearance of terms of lower than cubic symmetry (i. e., of axial symmetry with respect to the film normal) in the magnetic anisotropy energy associated with this change. The present paper considers the origin and nature of this additional axial anisotropy within the framework of the itinerant electron theory of magnetism. Within the localized-moment picture, as treated by Néel, this axial anisotropy is associated with effects occurring only at the surface planes, and therefore has come to be known as "surface anisotropy." We retain this nomenclature even though in our itinerant-electron picture the changes in anisotropy can be associated with electronic states extending into the interior of the film. The most striking qualitative result of our model is the marked variation of surface anisotropy with thickness possible for very thin films. This constrasts with the behavior in the Néel model, where for very thin films the surface anisotropy energy is almost independent of the film thickness. Physically this difference in behavior can be understood, since the itinerant-electron model allows the presence of coupling between the behavior at the two surfaces of the film, while such coupling cannot exist in the Néel model. We discuss the relevance of this difference to the existing experimental observations and to possible future experiments.

I. INTRODUCTION

The free energy of a ferromagnetic metal crystal depends on the direction of its magnetization with respect to the crystal axes. This anisotropy energy[1-6] can be measured by obtaining magnetization vs external-field curves for several directions of the applied field, by torque experiments, or by ferromagnetic resonance, and reflects both the sample's inherent crystal symmetry and its shape. For example, the observed free energy of a bulk cubic material such as Ni[1,7,8] or Fe[1,7] may be expanded in terms of cubic harmonics:

$$F(\alpha_1, \alpha_2, \alpha_3) = K_0 + K_1(\alpha_1^2\alpha_2^2 + \alpha_2^2\alpha_3^2 + \alpha_1^2\alpha_3^2) + K_2(\alpha_1^2\alpha_2^2\alpha_3^2) + \cdots , \quad (1.1)$$

where the α_i are the direction cosines of the magnetization with respect to the crystal axes.

A very thin crystal (i. e., single-crystal film) of a cubic metal such as nickel is no longer truly cubic, and this departure from cubic symmetry is reflected in the nature of the electronic states. One therefore anticipates the appearance of terms of lower than cubic (i. e., of axial symmetry) in the magnetic anisotropy energy. This is true in both the localized moment[6,9] and itinerant-electron[10] points of view. The present paper considers the origin and nature of this additional axial anisotropy within the framework of the itinerant-electron theory of magnetism. Within the localized-moment picture used by Néel,[6,9] this axial anisotropy is associated with effects occurring only at the surface planes, and therefore has come to be known as "surface anisotropy." We shall retain this nomenclature even though in our band treatment of the electronic structure the changes in anisotropy can be associated with electronic states extending into the interior of the film. In addition to the anisotropy effects caused by changes in the nature of the electronic states due to the intrinsically lower symmetry associated with the film geometry, experimentally there can be anisotropic contributions to the energy due to various impurity and stress effects associated with film growth. We shall concern ourselves here only with the intrinsic surface anisotropy. The other important source

of lower than cubic anisotropy, present even for a perfect thin film, is the classical demagnetization, or shape, anisotropy. We shall discuss the relative sizes and differences in behavior of the surface and shape anisotropies below.

For transition metals there have historically been two approaches to the problem of bulk magnetic anisotropy. One of these, followed by Van Vleck, [11] is based on the localized d-electron model, while the other, as used by Brooks[12] and by Fletcher, [13] is based on the band, or itinerant-electron, picture of the $3d$ electrons.

Van Vleck's phenomenological theory[11] of the bulk anisotropy of Ni and Fe was based on the presence of pseudodipolar and pseudoquadripolar coupling between the localized electron spins of the magnetic system. Since the classical dipolar and quadripolar interactions are much too small to explain the observed effects, phenomenological coupling constants were introduced to give order-of-magnitude agreement with experiment. (Van Vleck[11] suggested that the origin of this coupling was in the combined effect of orbital coupling and spin-orbit interaction.) Various spin-Hamiltonian calculations[14] of the magnetic anisotropy have been based on such pseudodipolar and pseudoquadripolar couplings.

In the itinerant-electron treatment of Brooks, [12] the spin-orbit coupling was also pictured as playing a key role in the origin of the bulk magnetic anisotropy energy. In Brooks's theory, however, the way in which spin-orbit coupling gave anisotropy was treated much less phenomenologically. The spin-orbit interaction was considered as a perturbation on the crystal potential giving the d-electron band states. The orbital parts of the electron-band wave functions have the symmetry of the crystal potential. The energy then depends on the direction of spin, and hence magnetization, with regard to the crystal axes, because the spin senses the symmetry of the crystal potential through the spin-orbit coupling.

The d-band wave functions in Brooks's theory were calculated in the tight-binding approximation, with the exchange effects which give rise to ferromagnetism being treated by an effective exchange splitting between up- and down-spin bands as in the Stoner collective-electron picture[15] of ferromagnetism. For a cubic metal such as Ni, the first anistropic contribution to the energy is obtained in fourth-order perturbation theory. Only the triply degenerate magnetically active $T_{2g}(\Gamma_5, \Gamma_{25'})$ level was considered by Brooks, but Fletcher[13] treated all the d states. Slonczewski[16] later considered the effect on the anisotropy of changes in occupation of states near the Fermi energy due to the spin-orbit coupling. Because of the sensitivity to details of the band structure, caused partially by the high order of perturbation theory used, the various calculations using the itinerant-electron modes give order-of-magnitude rather than detailed numerical agreement with experiment. They do, however, provide a nonphenomenological explanation of magnetic anisotropy – one suitable for itinerant ferromagnets.

Néel's[9] theoretical investigation of the surface anisotropy was phenomenological and similar to Van Vleck's approach[11] to the bulk problem. Néel suggested that the source of surface anisotropy was the difference between the environment (i.e., the positions of near neighbors) of the surface atoms and those of the bulk. A phenomenological, nearest-neighbor pseudodipolar interaction was used to predict the variation of the anisotropy with exposed surface. The magnitudes of the coupling constants were estimated from magnetostriction constants.

We consider here a less phenomenological approach to the surface anisotropy. Our calculations follow the general philosophy of Brooks[12] in that the anisotropy arises from treating the spin-orbit coupling as a perturbation on the itinerant-electron states (i.e., energy-band states for Brooks's bulk theory and the corresponding states in the film case as found in Ref. 10). Interference effects between the two film surfaces affect the symmetry of the electron states by allowing only certain discrete wave vectors. These states are in turn coupled to the magnetization direction by the spin-orbit coupling. If one ignores the change of various overlap integrals in the surface region, the difference between the tight-binding wave functions of a film and those of a bulk sample corresponds to the loss of translational and cubic symmetry. [10] Since the symmetry is no longer cubic, the spin-orbit coupling gives a net anisotropy in second-order perturbation theory. This anisotropy, of axial symmetry with respect to a film normal, is the surface anisotropy in the present treatment. As an example, we consider the surface anisotropy of Ni films, in a highly simplified picture of the band structure, with a $\langle 100 \rangle$ direction as normal.

The most striking qualitative result of our model is the marked variation of surface anisotropy with thickness possible for very thin films. This contrasts with the behavior in the Néel model, where for very thin films the surface anisotropy energy is almost independent of the film thickness.

II. CALCULATIONAL PROCEDURE

We have shown previously[10] that, within the tight-binding approximation, to each energy eigenvalue of a film there correspond values of an angular variable θ that itself corresponds to the product of wave vector times lattice parameter (ka) in the bulk limit. For the single-band situation for both

⟨100⟩ and ⟨111⟩ films, each energy eigenvalue corresponds to a single value of the magnitude of θ. Making the correspondence between θ and ka (with the appropriate phase shift in the ⟨111⟩ case), for a crystal of N layers, the N energy eigenvalues lie on top of the corresponding bulk band ($\vec{k}$ parallel the film normal) and are equally spaced in θ. For a ⟨100⟩ film with two or more interacting bands, this remains true. However, for a ⟨111⟩ film with two or more interacting bands the situation changes. In the absence of surface states, the film energy eigenvalues continue to fall on top of the bulk bands, but they are no longer evenly spaced in θ, and in general more than one value of θ corresponds to given energy.[10]

When the θ spacing is not periodic, its specification requires complicated calculations. We therefore confine our attention to ⟨100⟩ Ni films. In this ⟨100⟩ case, it is formally simple to include exactly all effects giving the departure from cubic symmetry which thereby lead to the presence of an axially symmetric magnetocrystalline anisotropy energy. All departures from cubic symmetry are embodied in the fact that the mesh spacing in $\vec{k}$ space is much greater parallel to the direction of thinness of the film than perpendicular to that direction. Following Brooks,[12] we consider only the threefold-degenerate $T_{2g}(\Gamma_5, \Gamma_{25'})$ d levels. To further reduce the length of numerical calculation, we treat here the case of the three noninteracting bands. This study is sufficient to illustrate the main qualitative features to be considered in formulating an experimental program. More realistic calculations for nickel which include band mixing and all d levels may be reported later.

We first review and extend some previous results[10] for the tight-binding wave functions of an N-layer film. The layers are each considered to be infinite in their two dimensions ($N_2, N_3 \to \infty$) and are treated using periodic boundary conditions. Our treatment is thus restricted to films in which $N < N_2, N_3$. The electron wave functions are taken to be linear combinations of the tight-binding functions within a layer. Assuming no interband mixing, we write

$$\Psi^{j\theta}_{p_2 p_3 s} = \sum_{l=1}^{N} S^{\theta}_{jl}\, \Psi^{l}_{j p_2 p_3}\, \zeta , \tag{2.1}$$

where j is a band index, s is a spin index with ζ the appropriate spinor, and

$$\Psi^{l}_{j p_2 p_3} = \left[\frac{2}{N_2 N_3 (N+1)}\right]^{1/2} \times \sum_{m=1}^{N_2} \sum_{n=1}^{N_3} \exp\left[i\left(\frac{2\pi p_2 m}{N_2} + \frac{2\pi p_3 n}{N_3}\right)\right] \times \varphi_j(\vec{r} - \vec{r}_{lmn}) \tag{2.2}$$

is the tight-binding wave function for the lth layer corresponding to the jth atomic d-wave function.

The quantities p_2/N_2 and p_3/N_3 (with p_2 and p_3 integers $\leq N_2$ and N_3, respectively) are good quantum numbers and label points in a two-dimensional Brillouin zone. The zone for the case of a ⟨100⟩ plane in an fcc lattice is shown in Fig. 1. The index θ is the effective quantum number in the direction perpendicular to the film.

The use of only nearest-neighbor overlap integrals in the Schrödinger equation

$$\langle \Psi^{j\theta}_{p_2 p_3 s} | \mathcal{H} - E | \Psi^{j\theta}_{p_2 p_3 s} \rangle = 0 \tag{2.3}$$

yields second-order difference equations for S^{θ}_{jl},

$$R_j S^{\theta}_{jl+1} + (F_j - E) S^{\theta}_{jl} + R_j S^{\theta}_{jl-1} = 0, \quad 2 \leq l \leq N-1. \tag{2.4}$$

If no change occurs in the overlap integrals near the surface, the boundary equations are given by

$$R_j S^{\theta}_{j2} + (F_j - E) S^{\theta}_{j1} = 0, \tag{2.5}$$

$$(F_j - E) S^{\theta}_{jN} + R_j S^{\theta}_{jN-1} = 0 . \tag{2.6}$$

The atomic T_{2g} wave functions serving as a basis for the noninteracting d bands are

$$\varphi_1(\vec{r}) = yz f(r), \quad \varphi_2(\vec{r}) = xz f(r), \quad \varphi_3(\vec{r}) = xy f(r), \tag{2.7}$$

and for an fcc crystal-structure film with a ⟨100⟩ normal,

$$F_1 = F_2 = 2A_2 \left[\cos(2\pi p_2/N_2) + \cos(2\pi p_3/N_3)\right] + E_0,$$

$$F_3 = -2A_1 \left[\cos(2\pi p_2/N_2) + \cos(2\pi p_3/N_3)\right] + E_0,$$

$$R_1 = -2A_1 \cos\left[\pi\left(\frac{p_2}{N_2} - \frac{p_3}{N_3}\right)\right]$$

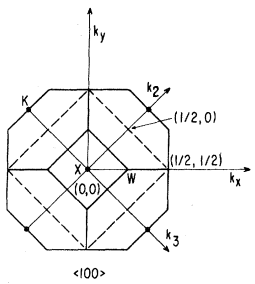

FIG. 1. Two-dimensional Brillouin zone for ⟨100⟩ plane of fcc lattice (dashed square) superimposed on a ⟨100⟩ view of the three-dimensional BZ for an fcc lattice. The $(p_2/N_2, p_3/N_3)$ coordinates for some of the symmetry points are as indicated. Note that in Ref. 10 the symmetry point K was inadvertently mislabeled.

$$+2A_2\cos\left[\pi\left(\frac{p_2}{N_2}+\frac{p_3}{N_3}\right)\right],$$

$$R_2=2A_2\cos\left[\pi\left(\frac{p_2}{N_2}-\frac{p_3}{N_3}\right)\right]$$

$$-2A_1\cos\left[\pi\left(\frac{p_2}{N_2}+\frac{p_3}{N_3}\right)\right], \qquad (2.8)$$

$$R_3=2A_2\cos\left[\pi\left(\frac{p_2}{N_2}-\frac{p_3}{N_3}\right)\right]$$

$$+2A_2\cos\left[\pi\left(\frac{p_2}{N_2}+\frac{p_3}{N_3}\right)\right],$$

where

$$A_1=-\int\varphi_3(x-\tfrac{1}{2}a,y-\tfrac{1}{2}a,z)[V-U]\,\varphi_3(x,y,z)\,d^3r, \qquad (2.9)$$

$$A_2=\int\varphi_3(x,y-\tfrac{1}{2}a,z-\tfrac{1}{2}a)[V-U]\,\varphi_3(x,y,z)\,d^3r\,.$$

Here $V-U$ is the difference between the crystal potential and that of an isolated atom, and a is the lattice constant. The parameter values for Ni,

$A_1=0.413$ eV,

$A_2=0.122$ eV,

$E_0=6.582$ eV,

are taken from the work of Hodges, Ehrenreich, and Lang.[17]

From the difference equation (2.4) one obtains the energy

$$E^{(0)}_{j\uparrow,\downarrow}=F_j+2R_j\cos\theta-(+)w, \qquad (2.10)$$

where we have assumed a rigid exchange splitting between the up- and down-spin bands, and $2w$ is the empirically determined exchange splitting equal to[17] 0.42 eV. The allowed values of θ and the coefficients S^{θ}_{jl} are determined from the boundary conditions, Eqs. (2.5) and (2.6), as

$$\theta_p=p\pi/(N+1),\quad p=1,2,\ldots,N \qquad (2.11)$$

$$S^{\theta}_{jl}=\sin l\theta\,. \qquad (2.12)$$

This expression for S^{θ}_{jl} gives the normalized eigenfunctions.

The spin-orbit interaction is given by

$$H_{SO}=\sum_{\vec{l}}\zeta(|\vec{r}-\vec{l}|)\;\vec{s}\cdot\vec{L}(\vec{r}-\vec{l}), \qquad (2.13)$$

where the $\vec{l}$ span the lattice sites in the crystal, and $\zeta(|\vec{r}-\vec{l}|)$ falls off rapidly with distance, If the interaction is assumed to connect only those atomic orbitals centered on the same site, the matrix elements of the spin-orbit Hamiltonian may readily be shown to be diagonal in p_2, p_3, and θ_p. One obtains

$$\langle\Psi^{j\theta}_{p_2p_3s}|\mathcal{H}_{SO}|\Psi^{j'\theta}_{p_2p_3s'}\rangle=A\langle\varphi_j\,s|\vec{s}\cdot\vec{L}|\,\varphi_{j'}\,s'\rangle, \qquad (2.14)$$

where A is the spin-orbit parameter[18] for free atoms ($A=0.0785$ eV for Ni). The spin-orbit matrix elements between the T_{2g} atomic wave functions are

$$\begin{aligned}
&\langle\varphi_{1\uparrow}|\vec{s}\cdot\vec{L}|\varphi_{2\uparrow}\rangle=-\tfrac{1}{2}i\cos\eta, && \langle\varphi_{1\downarrow}|\vec{s}\cdot\vec{L}|\varphi_{2\downarrow}\rangle=\tfrac{1}{2}i\cos\eta\,,\\
&\langle\varphi_{1\uparrow}|\vec{s}\cdot\vec{L}|\varphi_{3\uparrow}\rangle=\tfrac{1}{2}i\sin\xi\sin\eta, && \langle\varphi_{1\downarrow}|\vec{s}\cdot\vec{L}|\varphi_{3\downarrow}\rangle=-\tfrac{1}{2}i\sin\xi\sin\eta,\\
&\langle\varphi_{2\uparrow}|\vec{s}\cdot\vec{L}|\varphi_{3\uparrow}\rangle=-\tfrac{1}{2}i\cos\xi\sin\eta, && \langle\varphi_{2\downarrow}|\vec{s}\cdot\vec{L}|\varphi_{3\downarrow}\rangle=\tfrac{1}{2}i\cos\xi\sin\eta,\\
&\langle\varphi_{1\uparrow}|\vec{s}\cdot\vec{L}|\varphi_{2\downarrow}\rangle=\tfrac{1}{2}i\sin\eta, && \langle\varphi_{1\downarrow}|\vec{s}\cdot\vec{L}|\varphi_{2\uparrow}\rangle=\tfrac{1}{2}i\sin\eta,\\
&\langle\varphi_{1\uparrow}|\vec{s}\cdot\vec{L}|\varphi_{3\downarrow}\rangle=\tfrac{1}{2}[\cos\xi+i\sin\xi\cos\eta], && \langle\varphi_{1\downarrow}|\vec{s}\cdot\vec{L}|\varphi_{3\uparrow}\rangle=\tfrac{1}{2}[-\cos\xi+i\sin\xi\cos\eta],\\
&\langle\varphi_{2\uparrow}|\vec{s}\cdot\vec{L}|\varphi_{3\downarrow}\rangle=\tfrac{1}{2}[\sin\xi-i\cos\xi\cos\eta], && \langle\varphi_{2\downarrow}|\vec{s}\cdot\vec{L}|\varphi_{3\uparrow}\rangle=\tfrac{1}{2}[-\sin\xi-i\cos\xi\cos\eta].
\end{aligned} \qquad (2.15)$$

Here the z crystal axis is taken normal to the film; η is the polar angle of the magnetization with respect to the z axis; and ξ is the azimuthal angle with respect to the x crystal axis (which lies in the plane of the film).

Second-order perturbation theory may be used to obtain the effect of the spin-orbit mixing on the energies E_{js} of the six bands. To find the net axial anisotropy, this second-order perturbation must be summed over all filled states. An important

simplification in the calculations follows from the fact that, because we are dealing with a second-order perturbation of the energy, in summing over all filled states a nonzero contribution will occur only because of perturbations of a filled state by an unfilled one. The net axial anisotropic energy is given by

$$E_{\mathrm{An}}^{(2)}(\eta)=\sum_{\substack{\text{filled}\\ \text{states}}}\left[E_{1\uparrow}^{(2)}+E_{1\downarrow}^{(2)}+E_{2\uparrow}^{(2)}+E_{2\downarrow}^{(2)}+E_{3\uparrow}^{(2)}+E_{3\downarrow}^{(2)}\right], \tag{2.16}$$

with

$$E_{1\uparrow}^{(2)}=\frac{A^2}{4}\left\{\left[\frac{1}{\omega_{12}-2w}+\frac{1}{\omega_{13}-2w}\right]+\cos^2\eta\left[\frac{1}{\omega_{12}}-\frac{1}{\omega_{12}-2w}\right]\right\}, \tag{2.17a}$$

$$E_{2\uparrow}^{(2)}=\frac{A^2}{4}\left\{\left[-\frac{1}{\omega_{12}+2w}+\frac{1}{\omega_{23}}\right]+\cos^2\eta\left[-\frac{1}{\omega_{12}}+\frac{1}{\omega_{12}+2w}-\frac{1}{\omega_{23}}+\frac{1}{\omega_{23}-2w}\right]\right\}, \tag{2.17b}$$

$$E_{3\uparrow}^{(2)}=\frac{A^4}{4}\left\{\left[-\frac{1}{\omega_{13}+2w}-\frac{1}{\omega_{23}}\right]+\cos^2\eta\left[\frac{1}{\omega_{23}}-\frac{1}{\omega_{23}+2w}\right]\right\}. \tag{2.17c}$$

The $E_{i\downarrow}^{(2)}$ are obtained by replacing w by $-w$ in Eqs. (2.17). Here $\omega_{ij}=E_{is}^{(0)}-E_{js}^{(0)}$, and the $E_{is}^{(0)}$ are given by (2.10). We have made use of the fact that $E_{\mathrm{An}}^{(2)}(\eta)$ must be independent of ξ to simplify the calculation by putting $\xi=0$ in the spin-orbit matrix elements used to obtain (2.17).

When the energies of the interacting states (E_{js}, $E_{j's'}$) are such that $|E_{js}-E_{j's'}|\lesssim A$, the use of nondegenerate perturbation theory is no longer justified. The energy of the occupied lower-lying level E_L is given by

$$E_L=\tfrac{1}{2}\left\{E_{js}+E_{j's'}-\left[(E_{js}-E_{j's'})^2+4A^2\left|\langle\varphi_j s\left|\vec{\mathrm{S}}\cdot\vec{\mathrm{L}}\right|\varphi_{j'}s'\rangle\right|^2\right]^{1/2}\right\}. \tag{2.18}$$

We assume that the occupation of the states is not affected by the spin-orbit interaction; i.e., E_{js} and $E_{j's'}$ are, respectively, less than and greater than E_F, with or without spin-orbit interaction. Thus the Slonczewski[16] effect noted in Sec. I is not included here. (Only when the energies, including spin-orbit interaction, are such that $E_{js}<E_F<E_{j's'}$ will the summed contributions of such states be nonzero.)

The total energy of the occupied states is calculated in two approximations. The first approach (I) consists of using only the second-order perturbation theory given in Eqs. (2.16) and (2.17). When the interacting states are such that $E_{js}<E_F<E_{j's'}$ and $E_{j's'}-E_{js}\lesssim\alpha$, where α is of the order of the spin-orbit coupling parameter A, $E_{j's'}-E_{js}$ is set equal to α. (For most of the calculations α has been taken equal to A. However, for $N=4$, as discussed below, α has been varied somewhat about this value to check the sensitivity of the calculations to the choice of α.) The anisotropic term in the energy then is proportional to $\cos^2\eta$. In the second approach (II), such states are treated using Eq. (2.18) with E_{js} set equal to $E_{j's'}$. In this approach, in addition to the $\cos^2\eta$ term, the total energy also contains anisotropic contributions varying as $|\cos\eta|$ and $|\sin\eta|$. The total energy of the occupied states E_T may be expressed as

$$E_T^{\mathrm{I}}(\eta)=B+C\cos^2\eta \tag{2.19}$$

when calculated by the first method, and as

$$E_T^{\mathrm{II}}(\eta)=D+F\cos^2\eta+G|\cos\eta|+H|\sin\eta| \tag{2.20}$$

when calculated by the second method.

III. RESULTS AND DISCUSSION

The Fermi energy $E_F=0.3248$ eV corresponding to 3.85 occupied T_{2g} d states per atom is fixed by demanding that the difference between the number of up- and down-spin electrons per atom be 0.54, the approximate value in nickel. (As might be expected, the results given here do depend reasonably strongly on E_F.) For a fixed N (film thickness in number of atomic layers), the coefficients in (2.19) and (2.20) are calculated for various values of $N_2=N_3$ (film width). As N_2/N becomes large (~ 10), the values of the coefficients approach asymptotic values which characterize the N-layer film. Some fluctuations about the apparent asymptotic values occur. In general, computing-time restrictions limit identification of the asymptotic values to an accuracy of about 10%. The type of behavior found is illustrated in Figs. 2(a) and 2(b), where the variation with $N_2=N_3$ of the various coefficients of a three-layer $\langle 100\rangle$ film are shown for the first and second approaches of Sec. II, respectively.

We have investigated the variation of the axial anisotropy energy with film thickness for fixed film width using both the first approach giving the expression of Eq. (2.19) and the second approach giving (2.20). Both types of calculation were performed for films of 3 to 8 layers, while the first

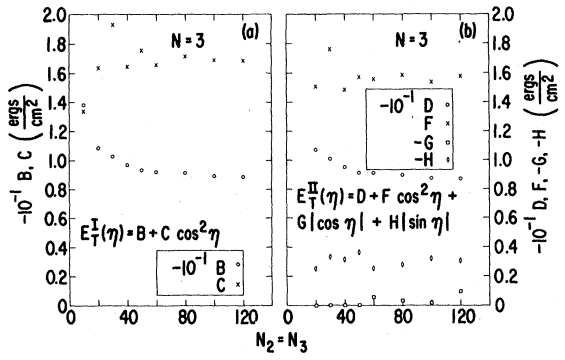

FIG. 2. (a) Variation of the energy coefficients defined in Eq. (2.19) with $N_2 = N_3$ for fixed $N = 3$. (b) Variation of the energy coefficients defined in Eq. (2.20) with $N_2 = N_3$ for fixed $N = 3$. The energies have been normalized to be per unit area of the film, and all coefficients are in erg/cm^2.

approach was used for thicknesses up to 17 layers. A simple but meaningful measure of the anisotropy given by the second approach is required. We choose for such a measure the difference in energy per unit area between magnetization parallel to the film and normal to the film:

$$K_{s1,2} \equiv E_T^{I,II}(\tfrac{1}{2}\pi) - E_T^{I,II}(0) \ . \qquad (3.1)$$

(Here the energy is normalized so that K_s has units of energy per unit area.) Both this surface anisotropy energy K_s and the individual coefficients defined in Eqs. (2.19) and (2.20) are given in Table I for fixed $N_2 = N_3 = 100$ and values of N up to 17 for method I and up to 8 for method II. The behavior shown in Table I is very similar to that which would be obtained using the large N_2 asymptotic values of the various coefficients and of K_s for each N. [For method I, the magnitude of K_s is always the difference between the extreme values of the energy. In method II, this is not always so, and $\eta = \frac{1}{4}\pi$ can give an extremum of energy. For $N = 6$ and 8 the minimum value of E_T^{II} occurs at $\eta = \frac{1}{4}\pi$ and the maximum at $\frac{1}{2}\pi$; and the value of $E_T^{II}(\frac{1}{2}\pi) - E_T^{II}(\frac{1}{4}\pi)$ is given in parentheses beside the tabulated K_{s2}.] As a check on the sensitivity to the choice of cutoff parameter α, the second approach was applied to the four-layer film using values of $\alpha = \frac{1}{2}A$ and $2A$. The results did not change significantly. In general, the anisotropies predicted by methods I and II are quite similar. This indicates that both are probably reasonable approximations to an exact calculation. (The fact that the isotropic terms, B and D as given in Table I, increase almost linearly with N is an indication of the accuracy of our numerical summation procedures.)

Figure 3 shows a plot of the K_{s1} and K_{s2} vs N behavior given in Table I. For very thin films ($N = 3, 4, \ldots, 8$) the sign of K_s oscillates. As N becomes larger ($N = 9, \ldots, 12$), the sign of K_{s1} (method I) appears to become negative, and the envelope amplitude becomes smaller. There is some indication ($N = 16$, 17, method I) that oscillations in the envelope persist to rather large values of N. The calculation for $N = 17$ requires approximately 1 h of Ge 600 computer time. As a result, thicker films were not investigated.

The origin of the surface anisotropy in our model lies in the symmetry restrictions imposed on the allowed electron states by the simultaneous presence of the two surfaces. The resulting discrete $\vec{k}$ mesh is, for small N, quite sensitive to the number of layers. The presence of oscillation in sign of K_s with N as shown in Fig. 3 depends on the detail of the band structure. For odd N, one fills in a different mesh in $\vec{k}$ space for $\vec{k}$ normal to the film

TABLE I. Energy coefficients, defined in Eqs. (2.19) and 2.20), and surface anisotropy energies [$K_{s1} \equiv E_T^I(\frac{1}{2}\pi) - E_T^I(0)$, $K_{s2} \equiv E_T^{II}(\frac{1}{2}\pi) - E_T^{II}(0)$] for fixed film width $N_2 = N_3 = 100$ and varying film thickness N in number of atomic layers. The energies have been normalized to be per unit area of the film, so all coefficients are in erg/cm^2. For $N = 6$ and 8, the minimum value of E_T^{II} occurs at $\eta = \frac{1}{4}\pi$ and the maximum at $\frac{1}{2}\pi$; for those cases the value of $E_T^{II}(\frac{1}{2}\pi) - E_T^{II}(\frac{1}{4}\pi)$ is given in parentheses besides the tabulated K_{s2}.

N	B	C	K_{s1}	D	F	G	H	K_{s2}
3	− 8.94	1.69	−1.69	−8.79	1.54	−0.002	−0.32	−1.86
4	−11.74	−1.49	1.49	−11.25	−1.55	−1.02	−1.15	1.42
5	−14.75	1.53	−1.53	−14.33	1.29	−0.23	−0.68	−1.74
6	−17.96	−0.54	0.54	−17.62	−0.48	−1.23	−1.11	0.60 (0.78)
7	−20.15	1.09	−1.09	−19.77	0.62	−0.31	−1.16	−1.46
8	−23.67	−0.10	0.10	−23.27	−0.10	−1.48	−1.41	0.16 (0.68)
9	−25.65	0.10	−0.10	...	...	...	...	...
10	−29.26	0.13	−0.13	...	...	...	...	...
11	−31.61	0.36	−0.36	...	...	...	...	...
12	−34.34	0.08	−0.08	...	...	...	...	...
13	−37.61	0.92	−0.92	...	...	...	...	...
16	−45.67	−0.57	0.57	...	...	...	...	...
17	−48.49	0.61	−0.61	...	...	...	...	...

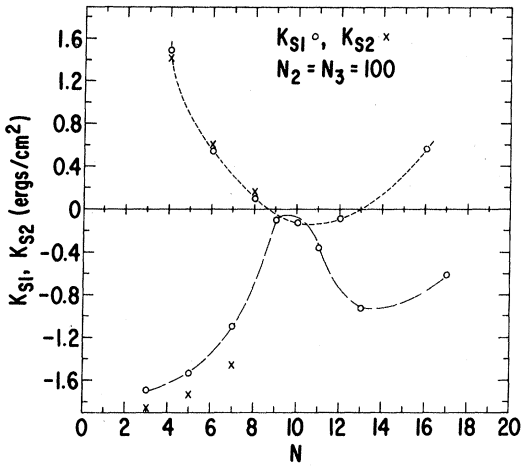

FIG. 3. Variation of the anisotropy energy per unit area [as defined in Eq. (3.1)] with film thickness N for fixed film width $N_2 = N_3 = 100$. K_{s1} and K_{s2} are, respectively, the results of the first and second methods of calculation. The short-dashed curve indicates the envelope of K_{s1} values for even N, and the long-dashed curve indicates the envelope for odd N.

than for even N, and such sampling differences are most important at small N. While such oscillations may not occur for all band structures, it is reasonable to expect this behavior to be fairly common.

The values of K_s characteristically fall in the range 0.1 – 1.0 erg/cm^2. (The value of K_s estimated using the Néel model is of about the same magnitude.) In practice, to observe the surface anisotropy energy requires separating it from the shape anisotropy resulting from classical demagnetization effects. For a thin film the shape anisotropy per unit area is

$$K_{\text{demag}} = Na\pi M^2. \tag{3.2}$$

Using $M = 508.8$ g for Ni and $a = 3.52$ Å gives $K_{\text{demag}} = 1$ erg/cm^2 for $N = 35$ and $K_{\text{demag}} = 0.1$ erg/cm^2 for N between 3 and 4. Thus for film thicknesses of a few tens of layers, the surface anisotropy can be comparable to, or larger than, the shape anisotropy. An important aid in separating out the surface anisotropy comes from the fact that the shape anisotropy for a thin film always tries to hold the magnetization in the plane of the film. On the other hand, for positive K_s the surface anisotropy favors alignment of the magnetization normal to the film.

In the years following Néel's original predictions, there have been a number[6] of attempts to observe surface anisotropy in various film and small-particle precipitate systems. The extent to which surface anisotropy has been observed is not clear.

One recent careful attempt to study surface anisotropy effects experimentally is the work of Goldmann and Müller[19] on single-crystal films of $Ni_{0.48}Fe_{0.52}$ (permalloy) with ⟨111⟩ normal, grown epitaxially on atomically flat Cu ⟨111⟩ films. The film thicknesses varied from 3 atomic layers up to about 200 layers. The behavior of the surface anisotropy with varying film thickness is somewhat obscured by the rather marked decrease of magnetization with film thickness. The magnetization for a 3-layer film is only about 40% of that for a 50-layer film, which is quite close to the bulk magnetization. If one evaluates the surface anisotropy using the actual magnetization values for the various thicknesses, the value of K_s increases from a little more than 0.1 erg/cm^2 for $N = 3$ to somewhat more than 1 erg/cm^2 for $N = 20$. If, on the other hand, as Goldmann and Müller suggest, one divides out the change in the square of the magnetization with thickness, the increase between $N = 3$ and 20 is about a factor of 2 rather than a factor of 10. (The surface anisotropy throughout the measured range favors magnetization alignment normal to the film.)

The question of the variation of surface anisotropy energy with film thickness is an important one meriting further careful study. The possibility of difference in this behavior is the main qualitative difference between the predictions of our itinerant-electron model and those of Néel's localized-moment treatment. Physically this difference in behavior can be understood since the itinerant-electron model allows the presence of coupling between the behavior at the two surfaces of the film, while such coupling cannot exist in the Néel model. This difference may help to explain some of the ambiguity in the past experimental situation with regard to the observation of surface anisotropy (besides the obvious experimental difficulties of making measurements on samples corresponding to "perfect slices" of single crystals), and at the same time suggests some very interesting, and probably difficult, possible experimental observations.

For very thin films (a few tens of atomic layers) in the Néel model one expects the surface anisotropy energy to be almost independent of the film thickness. On the other hand, in our itinerant-electron model, one can have very sharp changes in surface anisotropy energy for small changes in thickness. (See, for example, the change between large positive K_s as N varies between even and odd N for small N in Fig. 3.) One expects the nature of these changes to be sensitive to details of the band structure, so that one might have K_s decreasing, increasing, or oscillating rather sharply as N increases. This possibility of strong variation of K_s with N may explain some of the ambiguity in past observations (and, indeed, the absence of any observed K_s in some cases). Any real film would probably have some variation in N. If K_s oscillated rather sharply in sign with N, one could have considerable cancel-

lation so far as the total net anisotropy energy of the film were concerned. The observed value of K_s would then be quite sensitive to the detailed nature of the film. Our model calculations thus indicate potential, possibly severe experimental difficulties. On the other hand, there is great inducement to try to make films of a thickness specified, at least predominantly, within one atomic layer. We anticipate that the change in anisotropy on changing thickness by one atomic spacing might be very dramatic. Indeed, such experiments could provide a very sensitive probe of the changes in electronic structure with thickness of ferromagnetic metal crystals.

[1]R. M. Bozorth, *Ferromagnetism* (Van Nostrand, Princeton, N. J., 1951).
[2]C. Kittel, *Introduction to Solid State Physics*, 2nd ed. (Wiley, New York, 1953), Chap. 15.
[3]W. J. Carr, Jr., in *Handbuch der Physik*, edited by S. Flügge and H. P. J. Wijn (Springer-Verlag, Berlin, 1966), Vol. XVIII/2, pp. 274–340.
[4]J. Kanamori, in *Magnetism*, edited by G. T. Rado and H. Suhl (Academic, New York, 1963), Vol. I, Chap. 4.
[5]R. F. Soohoo, *Magnetic Thin Films* (Harper & Row, New York, 1965), Chap. 7.
[6]I. S. Jacobs and C. P. Bean, in *Magnetism*, edited by G. T. Rado and H. Suhl (Academic, New York, 1963), Vol. III, Chap. 6.
[7]H. Sato and B. S. Chandrasekhar, J. Phys. Chem. Solids 1, 228 (1957).
[8]G. Aubert, J. Appl. Phys. 39, 504 (1968).
[9]L. Néel, Compt. Rend. 237, 1468 (1953); J. Phys. Radium 15, 225 (1954).
[10]B. R. Cooper and A. J. Bennett, Phys. Rev. B 1, 4654 (1970).
[11]J. H. Van Vleck, Phys. Rev. 52, 1178 (1937).
[12]H. Brooks, Phys. Rev. 58, 909 (1940).
[13]G. C. Fletcher, Proc. Phys. Soc. (London) A67, 505 (1954).
[14]F. Keffer, in *Handbuch der Physik*, edited by S. Flügge and H. P. J. Wijn (Springer-Verlag, Berlin, 1966), Vol. XVIII/2, pp. 1–273.
[15]E. C. Stoner, Proc. Roy. Soc. (London) A165, 372 (1938).
[16]J. C. Slonczewski, J. Phys. Soc. Japan 17, 34 (1962).
[17]L. Hodges, H. Ehrenreich, and N. D. Lang, Phys. Rev. 152, 505 (1966); L. Hodges, Ph.D. thesis, Harvard University, 1966 (unpublished).
[18]C. Moore, *Atomic Energy Levels* (National Bureau of Standards, Washington, D. C., 1952), Vol. II.
[19]U. Gradmann and J. Müller, Phys. Status Solidi 27, 313 (1968).

PHYSICAL REVIEW B VOLUME 3, NUMBER 5 1 MARCH 1971

Magnetically Induced Electric Field Gradient at the Nucleus of High-Spin Fe^{2+} Ion in Distorted Cubic Crystal Field*

R. Kamal and R. G. Mendiratta
Department of Physics, Indian Institute of Technology, New Delhi-29, India
(Received 31 August 1970)

Calculations of a magnetically induced electric field gradient (EFG) at the nucleus of a high-spin Fe^{2+} ion in an axially distorted crystal field have been made. This was done by considering the secular problem of finding eigenstates and eigenvalues for the ground state Γ_5 of the Fe^{2+} ion in an axially symmetric crystal field and then by treating the interaction between magnetic terms of the total interaction Hamiltonian with the crystal field via spin-orbit coupling as a perturbation. It is observed that the principal component of the magnetically induced EFG increases nonlinearly with the crystal-field distortion and approaches a constant value at large values of distortion. It is also seen that the magnetically induced EFG is much more sensitive to temperature in a distorted crystal field than in a cubic field. Further, the sign of the magnetically induced EFG is found to be the same as that of the zero-order EFG. The experimental results of Mössbauer experiments in $RbFeF_3$ in its antiferromagnetic phase are also discussed.

I. INTRODUCTION

During the past few years, the knowledge of the electric-field-gradient (EFG) tensor has played an important role in determining many important properties in the field of nuclear, solid-state, and chemical physics. Until recently, nuclear quadrupole resonance spectroscopy was the main technique used in such studies. In recent years, Mössbauer spectroscopy has been very effectively used to measure the quadrupole splitting of the nuclear levels[1] and this gives useful information about the EFG at the nucleus. Using the crystal-field theory, several authors[2–4] have worked out the expressions for the EFG in various crystal-field symmetries around an iron nucleus. All these expressions give